

On the Density Probability Function of Galactic Gas. I. Numerical Simulations and the Significance of the Polytropic Index

John Scalo¹, Enrique Vázquez-Semadeni², David Chappell¹, and Thierry Passot³

¹*Astronomy Department, The University of Texas at Austin*

e-mail: `parrot,dwch@astro.as.utexas.edu`

²*Instituto de Astronomía, UNAM, Apdo. Postal 70-264, México, D. F. 04510, México*

e-mail: `enro@astroscu.unam.mx`

³*Observatoire de la Côte d'Azur, B.P. 4229, 06304, Nice Cedex 4, France*

e-mail: `passot@obs-nice.fr`

Submitted to *The Astrophysical Journal*.

ABSTRACT

We investigate the form of the one-point probability distribution function (pdf) for the density field of the interstellar medium using numerical simulations that successively reduce the number of physical processes included. Two-dimensional simulations of self-gravitating supersonic MHD turbulence, of supersonic self-gravitating hydrodynamic turbulence, and of decaying Burgers turbulence, produce in all cases filamentary density structures and evidence for a power-law density pdf with logarithmic slope around -1.7 . This suggests that the functional form of the pdf and the general filamentary morphology are the signature of the nonlinear advection operator.

These results do not support previous claims that the pdf is lognormal. A series of 1D simulations of forced supersonic polytropic turbulence is used to resolve the discrepancy. They suggest that the pdf is lognormal only for effective polytropic indices $\gamma = 1$ (or nearly lognormal for $\gamma \neq 1$ if the Mach number is sufficiently small), while power laws develop for densities larger than the mean if $\gamma < 1$. We evaluate the polytropic index for conditions relevant to the cool interstellar medium using published cooling functions and different heating sources, finding that a lognormal pdf may occur at densities between 10^3 and at least 10^4 cm^{-3} .

Several applications are examined. First, we question a recent derivation of the IMF from the density pdf by Padoan, Nordlund & Jones because a) the pdf does not contain spatial information, and b) their derivation produces the most massive stars in the *voids* of the density distribution. Second, we illustrate how a distribution of ambient densities can alter the predicted form of the size distribution of expanding shells. Finally, a brief comparison is made with the density pdfs found in cosmological simulations.

Subject headings: ISM: clouds – instabilities – magnetohydrodynamics – turbulence – STARS: IMF – cosmology

1. Introduction

In order for stars or groups of stars to form, densities must be sufficiently large, and so the statistical properties of the density field in the interstellar medium must be intimately connected with the star formation behavior of galaxies. The density field is coupled in a nonlinear manner to the velocity distribution of the gas, so the statistics of the density field can potentially serve as a diagnostic between different physical processes that might play a role in controlling the dynamics of interstellar material. For example, magnetically-dominated turbulence might exhibit significantly different density statistics than non-magnetic turbulence. Thus the density distribution could shed light on basic unsolved questions concerning star-forming regions, such as the nature and maintenance of highly supersonic motions observed at all but the smallest scales. The form of the density statistics might also be important in controlling the ability of galactic gas to spontaneously develop hierarchical structure, as suggested by Vázquez-Semadeni (1994). Padoan, Jones & Nordlund (1997) have shown how observations of extinction fluctuations by Lada et al. (1994) can be used to constrain the statistics of the density field, while Padoan (1995) and Padoan, Nordlund & Jones (1997) have attempted to relate the density distribution function to the stellar initial mass function, assuming a specific model for star formation. Understanding the physics behind the one-point density distribution function is also important in a cosmological context, since the form of this function in the nonlinear regime may be sensitive to the initial fluctuation statistics (see sec. 4.4. below).

In the present paper we focus on the behavior of the one-point probability distribution of gas densities in numerical simulations relevant to galactic gas. This function, denoted $f(\rho)$, is defined here such that $f(\rho)d\rho$ measures the fractional volume occupied by gas in the density range $(\rho, \rho + d\rho)$, so $f(\rho)$ is a probability density function (pdf) with units 1/density. If the density pdf is parameterized in some range of density as a power law with index θ , $f(\rho) \sim \rho^\theta$, then the fractional volume of space at density ρ per unit *logarithmic* density interval and the fractional *mass* of material per unit density interval would be a power law with index $(\theta + 1)$.

Vázquez-Semadeni (1994) presented evidence from two-dimensional numerical simulations of randomly-

forced turbulence that the density pdf may be lognormal in form; i.e. that the *logarithm* of the density has a probability density that is normal (Gaussian). However, his simulations were purely hydrodynamic (i.e., neglected self-gravity, the magnetic field and the Coriolis force), isothermal, and were restricted to relatively small Mach numbers compared to what is observed in most interstellar regions. Vázquez-Semadeni, Passot & Pouquet (1995) have presented simulations incorporating all of these physical effects, but discussed the density pdf only in passing. Nordlund & Padoan (quoted in Padoan et al. 1997a,b,c) have also found a lognormal density pdf in randomly forced isothermal three-dimensional simulations. These simulations include the magnetic field, and reach higher Mach numbers, but contain no other astrophysically relevant physical ingredients.

Part of the purpose of the present work is to examine whether this lognormal density pdf persists in simulations that include most of the major physical processes expected to play some role in galactic turbulence, including self-gravity, stellar heating, the magnetic field, rotation, and explicit heating and cooling functions in the energy equation, and which are carried out at large Mach numbers. If the results are different, we want to find out why, and try to isolate the dominant physical effect(s). In fact, Gotoh & Kraichnan (1993) have presented numerical evidence (and an interpretation in terms of the “mapping” closure) that the pdf for the Burgers equation (which is pressureless) is a power-law at high densities, rather than a lognormal.

In section 2.1 we first show that simulations of the most complex system do not result in a lognormal pdf, but instead show evidence for power law behavior at densities above the mean. In order to understand the reasons for the different result and to isolate the physical process(es) that are most responsible for this behavior, we next successively reduce the system by removing physical processes. In sec. 2.2 we examine simulations similar to the original set, but without magnetic fields and rotation. Again we find the power law pdf, with a similar slope and density range as before. As a more radical reduction of the system, in sec. 2.3 we study the density pdf for simulations that contain no physics at all except for nonlinear advection in the continuity and momentum equations (Chappell & Scalo 1997). These simulations contain no pressure, and so are equivalent to a gas with effective polytropic

index equal to zero.¹ Surprisingly, the spatial density fields and the density pdfs resemble the earlier simulations at densities above the mean, suggesting that advection is the dominant process. The importance of the advection term is well known in incompressible turbulence, in which even the pressure term can be incorporated into the nonlinear operator.

In order to understand these results, in section 3 we present a few conclusions that can be drawn from a large study of one-dimensional forced turbulence by Passot & Vázquez-Semadeni (1997), who have investigated the statistics of the density and velocity fields for a wide range of Mach numbers and polytropic indices. It turns out that a lognormal density pdf should only obtain at small Mach numbers or, for any value of the Mach number, when the polytropic index is equal to unity. This explains the discrepancy between the present simulations (all of which have small effective polytropic indices) and previous work (which assumed $\gamma = 1$). We also discuss the expected value of the polytropic index as a function of density and temperature, based on published cooling functions and various heating sources and conclude that at densities less than about 10^3 cm^{-3} the polytropic index should be significantly less than unity, favoring power-law density pdfs. For higher densities we show that saturation of the cooling function should lead to $\gamma \approx 1$ and therefore possibly a lognormal pdf. However at still larger densities γ gas-grain collisional cooling or heating should dominate, forcing γ away from unity again. Some implications of these results are discussed in section 4. In particular, we argue that the distribution of masses of collapsing structures or stars (the IMF) cannot be derived from the one-point density pdf, and illustrate how a distribution of densities might affect the predicted size distribution of expanding shells driven by young stars.

2. Three types of simulations and their pdfs

2.1. Self-gravitating magnetohydrodynamic models with rotation

A first class of models considered in the present paper consists of the fully nonlinear self-gravitating magnetohydrodynamic (MHD) equations with added

¹The polytropic index characterizes the response of the gas to quasi-static compression or expansion in thermal equilibrium, and is of course different from the ratio of specific heats which is, for example, 5/3 for a monotonic gas with no internal degrees of freedom.

model source terms for radiative cooling, stellar and diffuse heating, and the Coriolis force, as described in Passot, Vázquez-Semadeni & Pouquet (1995). The equations of this model, to which we will refer as the MHD model, are:

$$\frac{\partial \rho}{\partial t} + \nabla \cdot (\rho \mathbf{u}) = \mu \nabla^2 \rho, \quad (1)$$

$$\begin{aligned} \frac{\partial \mathbf{u}}{\partial t} + \mathbf{u} \cdot \nabla \mathbf{u} = -\frac{\nabla P}{\rho} - \left(\frac{J}{M_a}\right)^2 \nabla \phi + \\ \frac{1}{\rho} (\nabla \times \mathbf{B}) \times \mathbf{B} - 2\Omega \times \mathbf{u} - \nu_8 \nabla^8 \mathbf{u} + \\ \nu_2 (\nabla^2 \mathbf{u} + \frac{1}{3} \nabla \nabla \cdot \mathbf{u}) \end{aligned} \quad (2)$$

$$\begin{aligned} \frac{\partial e}{\partial t} + \mathbf{u} \cdot \nabla e = -(\gamma - 1)e \nabla \cdot \mathbf{u} + \kappa_T \frac{\nabla^2 e}{\rho} + \\ \left(\frac{1}{\rho}\right)(\Gamma_d + \Gamma_s - \Lambda), \end{aligned} \quad (3)$$

$$\frac{\partial \mathbf{B}}{\partial t} = \nabla \times (\mathbf{u} \times \mathbf{B}) - \nu_8 \nabla^8 \mathbf{B} + \eta \nabla^2 \mathbf{B}, \quad (4)$$

$$\nabla^2 \phi = \rho - 1, \quad (5)$$

$$P = (\gamma - 1)\rho e, \quad (6)$$

$$\Gamma_d(\mathbf{x}, t) = \Gamma_o(\rho/\rho_{ic})^a, \quad (7)$$

$$\Gamma_s(\mathbf{x}, t) = \begin{cases} \Gamma_1 \rho & \text{if } \rho(\mathbf{x}, t_0) > \rho_{cr} \\ & \text{and } 0 < t - t_0 < \Delta t_s, \\ 0 & \text{otherwise} \end{cases} \quad (8)$$

with

$$\Lambda = \rho^2 L(T), \quad (9)$$

and

$$L(T) = L_i T^{b_i} \quad \text{for } T_i \leq T < T_{i+1}, \quad (10)$$

where

$$\begin{aligned} T_1 &= 100 & L_1 &= 1.14 \times 10^{15} & b_1 &= 2 \\ T_2 &= 2000 & L_2 &= 5.08 \times 10^{16} & b_2 &= 1.5 \\ T_3 &= 8000 & L_3 &= 2.35 \times 10^{11} & b_3 &= 2.867 \\ T_4 &= 10^5 & L_4 &= 9.03 \times 10^{28} & b_4 &= -0.65 \\ T_5 &= 4 \times 10^7. \end{aligned}$$

We refer the reader to Passot et al. (1995) and to Vázquez-Semadeni, Passot & Pouquet (1996) for a detailed discussion of this model. Here we just describe it briefly. The numerical method used for solving these equations, as well as the purely hydrodynamic (HD) runs discussed in §2.2, is pseudospectral, implying that diffusion operators have to be included

explicitly, since the method does not produce any numerical viscosity. The initial conditions are Gaussian with random phases and a spectrum of the form $P(k) \propto k^4 \exp(-k^2/16)$ in all variables. All the simulations presented in this section are two-dimensional (2D).

In the momentum equation, eq. (2), Ω is the angular velocity of Galactic rotation, appearing in the Coriolis term, and ν_8 is a hyperviscosity coefficient also used in the magnetic flux freezing equation, eq. (4). The usage of hyperviscosity of the form ∇^8 instead of a standard Laplacian viscosity operator confines viscous effects to the very smallest scales in the simulations, allowing the development of larger turbulent inertial ranges. However, it produces oscillations in the vicinity of strong shocks, as discussed in §3.1, and thus a small amount of second-order viscosity has been added in some runs. A mass diffusion term, with a corresponding coefficient μ , is used in the continuity equation, in order to smooth out the density gradients, thus allowing the simulations to reach higher r.m.s. Mach numbers. A table with the full list of fiducial parameter values is presented in Passot et al. (1995).

In the internal energy equation, the terms Γ_d and Γ_s respectively refer to diffuse background and stellar heating rates per unit volume. The latter mimics the heating by ionization occurring in the HII regions surrounding OB stars, which are modeled as point heating sources appearing at every location where the density exceeds a threshold which we arbitrarily set at a density $\rho_c = 30\langle\rho\rangle$. The “stars” have a lifetime of 6.5×10^6 yr. Finally, Λ parameterizes the radiative cooling rate per unit volume. Note that, for compatibility with standard notation, we have changed the notation from that in Passot et al. (1995) and Vázquez-Semadeni et al. (1996). In those papers, Γ_s , Γ_d and $\rho\Lambda$ were the heating and cooling rates per unit *mass*, and the exponent in the equation defining Γ_d was labeled α , being related to the exponent used in the present paper by $a = 1 - \alpha$.

Figure 1 shows a typical view of the density field for one MHD two-dimensional (2D) simulation at a resolution of 800×800 grid points at time $t = 1.2t_o$, where $t_o = 8.2 \times 10^7$ yr is the sound crossing time for the integration domain. In this run, the dissipation coefficients are $\nu_8 = 5.63 \times 10^{-18}$, $\nu_2 = \eta = 0$, $\mu = 3.28 \times 10^{-3}$, and $a = 1/2$. The box size corresponds to a region of size 1 kpc in the Galactic plane at the solar galactocentric distance. We refer to this

simulation as MHD800. It is actually a restart of the run named “run 28” in Passot et al. (1995), but at larger resolution (run 28 had 512×512 grid points). Moreover, the star formation has been turned off in the last stages of this simulation in order to allow the turbulence to develop larger density peaks. Otherwise, the star formation criterion, which turns on a star whenever the density exceeds ρ_c , tends to prevent the simulation from reaching densities significantly higher than ρ_c , since the stars heat their surroundings, increasing the pressure and producing expanding bubbles, and reducing the density. This run is discussed in Vázquez-Semadeni, Ballesteros-Paredes & Rodríguez (1997), where another view of the density field at $t = 0.9t_o$ is presented. Note that the only stellar energy injection considered is that due to ionization heating of the medium surrounding OB stars, supernova explosions not being included. The latter implies that the largest complexes (see below) cannot be blown apart by the “stars”.

The density field is seen to consist of dense, filamentary, knotty structures (“clouds”) which are interconnected in extremely complicated patterns (“complexes”), being the local peaks within less dense, extended yet highly amorphous larger structures (“diffuse clouds”) (e.g., the two large structures in the upper- and lower-right parts of the figure). In turn, the diffuse clouds gradually disappear into the lowest-density “intercloud medium” (dark regions in the middle and left upper and lower parts of the image).

Figures 2a and 2b respectively show the histograms of $\log \rho$ ($= \rho f(\rho)$, where f is the density pdf), for run MHD800 at two different times, $t_1 = 0.9t_o$ and $t_2 = 1.2t_o$, the latter corresponding to the image shown in fig. 1. The density is shown in units of the mean density in the field. The histogram is computed over the whole field, so it contains 800^2 sample points.

The histogram at t_1 exhibits a clear power-law behavior in the interval $0 < \log \rho < 1.3$, with slope -0.73 . The histogram at t_2 , on the other hand, does not exhibit such a clear power-law behavior, although the region $0 < \log \rho < 1.5$ can be roughly approximated by a power-law of slope -0.63 . Both power-laws are indicated by the solid lines. Note that these slopes correspond to density pdfs f with slopes steeper by one power of ρ , i.e., $f \propto \rho^{-1.7}$.

For densities outside the ranges mentioned above, both histograms turn over, decaying rapidly at both very large and very small densities. The drop-off at large densities can be easily understood as a conse-

quence of the viscosity and mass diffusion included in the equations (the ν_8 and μ terms in eqs. [2] and [1], respectively), whose effect is to smooth out tall, narrow density peaks, “losing” them from the histogram. We speculate that the self-similar range would extend further into higher density values if more resolution (and consequently lower dissipative coefficients) could be used.

The turnover at low densities occurs close to the mean density, but has a much more abrupt character than either the Burgers’-type runs discussed in § 2.3 or the one-dimensional (1D) simulations of Passot & Vázquez-Semadeni, discussed briefly here in § 3.1. This is probably due to the presence of self-gravity in run MHD800, which has managed to collect the gas in large complexes, from which the gas cannot escape. Therefore, the gas in the voids is only slowly gravitationally accreted into the complexes, but cannot be swept up by the filaments as in the Burgers and 1D runs. That is, the density minima in run MHD800 are probably of gravitational, not turbulent origin, thus taking much longer times to be evacuated.

2.2. Hydrodynamic self-gravitating runs

In this section we briefly discuss a first simplification step down from the full eqs. (1) to (5), obtained by eliminating the magnetic field and the Coriolis force due to Galactic rotation in the simulations. This is an important case, because these physical agents can be the source of added “hardness” in the flow (§3.2; see also Vázquez-Semadeni et al. 1996).

Figures 3a and 3b show the density field for a 2D run (labeled HD512) similar to run MHD800 except without magnetic fields or the Coriolis force, and at a resolution of 512 grid points per dimension. At this lower resolution, the values of the diffusion parameters are $\nu_8 = 10^{-16}$, $\nu_2 = 2 \times 10^{-3}$, $\mu = 8 \times 10^{-3}$, and $a = 1/2$. The run considered evolves in time as follows. The initial turbulent transients induce the formation of clumps and filaments, which over the first 0.48 crossing times of the simulations ($= 3.9 \times 10^7$ yr) merge into larger and denser structures due to the combined action of turbulence and self-gravity but with no star formation activity. After this period, star formation begins, producing isolated expanding “HII regions”. However, since no supernovae are included, the stellar energy input is insufficient to halt collapse of the large structures, and by $t = 1.55t_o$, the largest structure finally collapses. Note that this type of collapse did not occur in the simulations of

Vázquez-Semadeni, Passot & Pouquet (1995), which were also non-rotating and non-magnetic, because the density threshold for star formation used in that paper was much lower ($8\langle\rho\rangle$) and the fluid was harder ($a = 1$).

The density field is shown at $t = 0.4t_o$ (fig. 3a) and $t = 1.47t_o$ (fig. 3b). The first time corresponds to an epoch shortly after the initial transients, at which matter has not significantly gathered gravitationally, and star formation events have not yet begun. The corresponding histogram for $\log \rho$ for this epoch is shown in fig. 4a, and contains 512^2 data points. Again a near power-law with slope ~ -0.6 can be seen in the range $-0.7 < \log \rho < 0.4$. Interestingly, at larger densities ($0.4 < \log \rho < 1.5$) another power-law can be fitted, with slope ~ -2.0 . Thus, power-law ranges in the density pdf appear to be present even after the removal of magnetic fields and rotation.

The density field shown in fig. 3b corresponds to the final state of run HD512, in which a large structure has collapsed gravitationally in the upper left quadrant of the field. The maximum density for this field, occurring at the center of the collapse, is $\rho = 703\langle\rho\rangle$. The corresponding histogram for $\log \rho$ is shown in fig. 3b. Quite surprisingly, even for this highly singular density configuration, the $\log \rho$ histogram exhibits a power-law range, although with two significant bumps at $1 < \log \rho < 1.5$ and at $2.5 < \log \rho < 2.75$. These bumps thus seem to correspond to two special densities: the density threshold for star formation (recall $\rho_c = 30\langle\rho\rangle$), and the density of the collapsed region. The bump at ρ_c can be easily understood since the stellar heating tends to prevent the density from exceeding ρ_c , except when the self-gravity of the complex is so large that the stellar heating is insufficient to prevent generalized collapse. Note again that this would not occur if supernovae capable of blowing away the complex were included. Nevertheless, the rest of the histogram continues to be a power-law. The measured slope is -1 . Thus, the power-law behavior at large densities is preserved in the absence of magnetic fields and rotation, and even in the presence of local gravitational collapse events.

2.3. Stripped-down quasi-Burgers simulations

A third series of simulations was run with the intention of stripping-down the momentum equation to isolate the effects of the advection term $\mathbf{u} \cdot \nabla \mathbf{u}$ in the momentum equation. For this purpose the equations of continuity and momentum conservation were

solved, but all terms on the RHS of the momentum equation were set to zero, except for an additional stellar forcing term equivalent to that used in the MHD and HD simulations. Both forced and decaying simulations were performed. Thus these calculations describe a highly compressible fluid in which advection and the corresponding “ram pressure” completely dominate the thermal pressure, or, equivalently, in which the effective polytropic index γ is zero. The system is equivalent to a forced Burgers flow, except that the viscosity in our case is numerical diffusion and the forcing is coupled spatially to the density field, since star formation and momentum input are assumed to occur at a threshold density. However, the runs with threshold star formation were not capable of generating a sufficiently broad range of densities at the high density end to learn much about the pdf, so we forego any discussion of the forced cases and consider only the pure decay simulations. The runs with star formation (most of the runs) will be discussed elsewhere (Chappell & Scalo 1997). Because of the similarity to Burgers turbulence, we refer to these simulations as series “B,” or “quasi-Burgers” runs.

The advection terms were differenced according to a variant of a Van Leer (1977) first-order scheme, altered to eliminate most of the spurious anisotropy of numerical diffusion in that scheme. The boundary conditions were doubly-periodic. The initial conditions were a uniform density field and a Gaussian velocity field with prescribed power spectrum. Runs with resolution of 128^2 , 256^2 , and 512^2 were examined. The scales were normalized such that the lattice spacing was 7.8 pc, so these resolutions correspond to a total region size of 1, 2, and 4 kpc, although the adopted size normalization is probably irrelevant for the results presented here concerning the density pdf. For pure advection, the hydrodynamic equations are invariant with respect to a change of scale, so these simulations can be applied to any scale.

All the simulations develop into a network of irregularly shaped filaments which cover a range of sizes. These filaments are the products of the advection operator nonlinearly self-organizing the initially randomized velocity field into a collection of shocks. The thicknesses of the filaments are set by numerical diffusion; they are thinner than in the MHD and HD cases because there is no pressure force. It is just this absence of pressure that ensures the larger compressibilities that feed the filament-generating advection

operator. With no momentum input, the filaments simply continue to sweep up material and each other, so that as time proceeds the structure becomes more concentrated on large scales and the velocities monotonically decrease. An image of the density field (actually of $\rho^{1/2}$) at two times is shown in Fig. 5. It is seen that the structure resembles the HD simulation shown in Fig. 3a at a time early enough that self-gravity has not yet caused the filaments to become concentrated into “complexes.”

Figure 6 shows the development of the density pdf (actually $\rho f(p)$) for two sets of 256^2 simulations, for initial conditions with velocity energy spectra proportional to k^{-2} (left) and k^0 (right). Each pdf is based on about 10^5 points, but most of them are in the voids between the filaments. The solid line is a reference lognormal pdf with peak at $\rho = 1$, shown just to illustrate the degree to which the simulation pdfs do or do not match a lognormal. Times are, from top to bottom, in units of initial crossing times, 0.006, 0.07, 1.1, and 17. After about 1 crossing time one can see the same sort of power law for $\log \rho \gtrsim 0$ that was found in the MHD and HD simulations. For both sets of initial conditions the logarithmic slope in the density is about -0.7 . The pdfs become noisy at late times because the density field has evolved into a relatively small number of large scale filaments. Although the number of points is too small to reveal the nature of the highest-density tail, the dropoff seen in the k^{-2} case, and to a lesser extent in the k^0 case, is consistent with the behavior seen in the better-sampled MHD and HD pdfs; the dropoff at highest densities is once again probably due to viscosity, which smears out the smallest scale structures, which are the thinnest, densest filaments that have recently undergone a collision with another filament.

We place no physical significance on the low density ($\rho \lesssim 1$) part of the pdf. In this pseudo-Burgers flow filaments sweep up all the inter-filament material, and once the entire simulation area has been crossed by at least one filament the density between filaments would be zero except for the action of viscosity (numerical diffusion here) which causes material to leak back into the “voids.” The low-density pdf extends to much lower densities than shown in the figure.

Figure 7 shows the late-time pdfs for three 256^2 simulations initially excited at a single given wavenumber $k_0 = 64$, 16, or 4. Although the impression is subjective, it appears that the pdfs are better represented, for $\rho \gtrsim 2$, by a power law plus a steeper

dropoff at large densities. The “knee” that separates the power-law density range from the dropoff appears to shift towards lower densities with increasing k_0 , occurring at $\rho \approx 60$ for $k_0 = 4$ and $\rho \approx 30$ for $k_0 = 16$. In both cases the logarithmic slope of the power law is around -0.6 to -0.8 . For $k_0 = 64$ the pdf appears to be fit by the lognormal for $\rho \gtrsim 2$, but inspection of other plots for this case at different times suggests that the knee has moved to such small densities, $\rho \sim 10$, that the power law region above $\rho \approx 2$ spans too small a range to be clearly visible. The knee in the $k_0 = 64$ case becomes more prominent at times later than shown in Fig. 7. This is because, when the initial velocity fluctuations have such a small scale, it takes many filament interactions to build up large structures. The same effect can be seen in Fig. 6 where the power law develops much earlier for the k^{-2} initial energy spectrum than for the k^0 spectrum.

In order to increase the sampling of cells at large densities, we ran a 512^2 simulation with a broad-band initial spectrum. The resulting density pdf is shown in Fig. 8 at two times. At early times the pdf at densities greater than the average appears to fit a lognormal, but after about 1.5 crossing times the result is more suggestive of a short power law segment with a falloff at $\rho \gtrsim 10$. Between $\log \rho = 0.2$ and 1.0 the logarithmic slope is about -0.6 .

We note that Gotoh and Kraichnan’s (1993) 1-dimensional simulations of the decaying Burgers equation produced a density pdf with a clear power-law form, although steeper than found here. Their power law regime had a larger extent in density probably because of the much greater dynamical range possible in 1D compared to the present 2D simulations. We take their work as support for the power law pdf regimes suggested here.

Because of the poor sampling statistics for these quasi-Burgers decay simulations compared to the MHD and HD runs, the results are not conclusive, but the pdfs are generally consistent with the power law segment plus high density falloff found in the more physically complete MHD and HD simulations. The rough agreement is especially surprising because the B simulations used a very different numerical method and, in most cases, different initial conditions. Since the B simulations have omitted all the physics except for nonlinear advection, this rather surprising agreement suggests that *the physical process responsible for the power law portion of the pdf in the high-density side*

is nonlinear advection. Intuitively, this can be understood in terms of the tendency of the advection term to induce multiplicative processes which may lead to power laws, if the equation of state permits it (Passot & Vázquez-Semadeni 1997, hereafter PVS).

3. The Role of the Polytropic Index

3.1. One-dimensional simulations

The simulations discussed in the previous sections suggest (with varying degrees of precision) the development of power-law regions at high densities in the density pdf of interstellar gas. This result is in contrast with previous work (Vázquez-Semadeni 1994; Padoan et al. 1997a,b,c) finding lognormal distributions in a variety of numerical simulations. Vázquez-Semadeni (1994) presented isothermal ($\gamma = 1$) simulations of two-dimensional, randomly-forced Navier-Stokes turbulence in the weakly compressible regime. No other processes, such as star formation, self-gravity, magnetic fields, etc., were included. Padoan et al. (1997a, b, c) refer to highly-compressible three-dimensional isothermal MHD simulations with random forcing and without self-gravity to be presented elsewhere, although, to our knowledge, the pdfs have not been published yet. For both sets of simulations, a lognormal pdf is reported.

The discrepancy between our pdfs and those of Vázquez-Semadeni (1994) and Padoan et al. (1997a,b,c) can be understood in terms of some recent results by PVS, which we briefly summarize here. As a first step towards understanding the relation between the dynamical and statistical properties of highly compressible turbulent flows, PVS have performed a systematic investigation of one-dimensional (1D) simulations of pure Navier-Stokes polytropic turbulence (with mass diffusion added on some runs in order to allow the simulations to tolerate strong shocks), finding that *a lognormal density pdf only appears when $\gamma = 1$.* In fact, as explained below, PVS suggest that the case $\gamma = 1$ may be singular in this respect.

The equations solved by PVS in nondimensional form are:

$$\frac{\partial \rho}{\partial t} + \frac{\partial(\rho u)}{\partial x} = \mu \frac{\partial^2 \rho}{\partial x^2}, \quad (11)$$

and

$$\frac{\partial u}{\partial t} + u \frac{\partial u}{\partial x} = -\frac{1}{\gamma M^2 \rho} \frac{\partial \rho^\gamma}{\partial x} + \nu_2 \left(\frac{\partial^2 u}{\partial x^2} \right) + a_r, \quad (12)$$

where M is the Mach number of the velocity unit.

In these simulations, only second-order viscosity is used in order to avoid the spurious oscillations induced in the vicinity of shocks by the use of hyperviscosity (Passot & Pouquet 1988). Mass diffusion (the RHS of eq. [11]) is used in small amounts to help the simulations survive strong shocks. The probability distributions of $\log \rho$ are obtained by considering all grid points (typically 2048) and averaging over nearly 150 code non-dimensional time units, sampling every 0.1 time units. Thus, the histograms contain over 3 million points.

As an illustration, we show in figs. 9a, and b the density fields of two different simulations, both with $M = 3$, and $\nu_2 = \mu = 0.003$, but with $\gamma = 1$ in (a) and $\gamma = 0.3$ in (b). These runs start at rest, but are driven with a random acceleration a_r at wavenumbers 2–20, with a correlation time $t_{\text{corr}} = 4.8 \times 10^{-4} t_o$. The associated histograms for $\log \rho$ are shown in figs. 10a and b. The dotted lines show a least-squares fit to a lognormal curve. As can be seen, for the simulation with $\gamma = 1$ the fit is excellent, suggesting that indeed the $\log \rho$ histogram is a true lognormal. Instead, in figure 10b, a clear power-law tail is seen to develop at large density fluctuations. Furthermore, in fig. 11 we show the corresponding histogram for a run with $\gamma = 0.3$ but $M = 1.8$. Upon comparison with fig. 9b, this run illustrates the effect of varying the Mach number M at a fixed γ . The deviation from a lognormal towards a high-density power-law tail is more noticeable at large M . These results are consistent with the power-law functional form of the pdf at high densities found by Gotoh & Kraichnan (1993) in their 1D numerical simulations of decaying Burgers turbulence, which effectively have $\gamma = 0$. Also, note that the development of the high-density power-law tail in the pdfs of the present simulations cannot be attributed to a numerical effect, such as the inclusion of the mass diffusion term in the continuity equation. Runs at lower Mach numbers (not shown), which could be performed without the need for such a term, still exhibited a power-law tail, although not as well developed, due to the Mach number dependence discussed above.

In order to interpret these results, it is instructive to rewrite the inviscid one-dimensional gas dynamics equations in Riemann invariant form. The Riemann invariants of the problem are defined, for $\gamma \neq 1$, as $z^\pm = u \pm Kc$, where u is the one-dimensional fluid velocity, $c = \rho^{(\gamma-1)/2}/M$ is the sound speed, and $K = \pm 2/(\gamma - 1)$. They are just advected along the

characteristics whose speeds are $u \pm c$. In the case $\gamma = 1$, $z^\pm = u \pm \log \rho/M$ while the characteristic speeds are $u \pm 1/M$. One can easily see that, under the transformation $\rho \rightarrow 1/\rho$, $\gamma \rightarrow 2 - \gamma$, the characteristic speeds remain unchanged while the Riemann invariants are exchanged. Under such a transformation the local dynamics is not preserved but the statistical quantities such as the pdf remain close. For $\gamma = 1$ this indication is consistent with the fact that the pdf is a lognormal, a curve symmetric under the change $\log \rho \rightarrow -\log \rho$.

It should be noted that the lognormal pdf at $\gamma = 1$ disappears when a random force f_r is used, leading to replace a_r by f_r/ρ in eq. (12). We speculate that this is due to the strong nonlinearity introduced by the division by ρ . Thus, to study the effect of the advection operator on the density pdf, the usage of an acceleration seems more adequate.

In terms of these results, we can interpret the previous claims of lognormal pdfs (Vázquez-Semadeni 1994; Padoan et al. 1997a,b,c) in a simple way. Since both sets of simulations were isothermal, their resulting pdfs were bound to be lognormal, independently of the Mach number. However, for any other values of the polytropic exponent, power-law pdfs should be realized.

3.2. The polytropic index of cool interstellar gas

The one-dimensional calculations of supersonic Navier-Stokes turbulence discussed above and presented in detail by PVS strongly suggest that the form of the density pdf $f(\rho)$ depends sensitively on the effective polytropic index γ . In particular, if the turbulence is highly supersonic, $f(\rho)$ is strictly lognormal only for γ equal to unity, while for smaller (larger) γ a power law develops for densities larger (smaller) than the mean. The sensitivity of hydrodynamic behavior to γ has been found previously in non-turbulent contexts. For example, Pongracic (1994) and Foster & Boss (1996) showed that the ability of a shock incident on a model cloud to induce gravitational collapse depends on γ (through a piecewise power law cooling rate for Pongracic). Vázquez-Semadeni et al. (1996) estimated a critical value of the polytropic exponent below which turbulence can induce bound condensations, as a function of the dimensionality of the turbulent compressions.

The polytropic index γ defined by $P \sim \rho^\gamma$, is iden-

tically zero for the quasi-Burgers simulations. For hydrodynamic simulations which allow for heating and cooling, γ can be determined locally by the temperature and density dependence of the heating and cooling function. If the heating and cooling rates per unit volume depend on temperature and density according to $\Gamma \sim \rho^a$ and $\Lambda \sim \rho^c T^b$, then the condition of thermal equilibrium (which holds for the flows of interest because of the small cooling times, except for just behind shocks), gives

$$\gamma = 1 + \frac{\partial \log T}{\partial \log \rho} = 1 - \frac{(c-a)}{b} \left(1 - \frac{\log \rho}{b} \frac{\partial b}{\partial \log \rho} \right) \quad (13)$$

(cf. Elmegreen 1991; Passot et al. 1995; Vázquez-Semadeni et al. 1996). The last factor in parentheses allows for the possibility that the temperature dependence exponent b in the cooling function is itself a continuous function of the density (see eq. [14] below).

In the MHD and HD simulations discussed above, the heating was assumed to be due to a combination of stellar and diffuse radiative heating, with $a = 0.5$ for the latter, while the cooling rate was a piecewise power-law function appropriate to temperatures larger than a few hundred degrees, because the simulations were designed to model large-scale dynamics of the atomic gas. For those simulations the values of γ are in the range 0–0.5.² Therefore the development of the power law $f(\rho)$ at large densities found in the MHD, HD, and B simulations is consistent with the one-dimensional results, since γ is significantly smaller than unity.

However, the most interesting applications of the density pdf concern regions that can form stars, which are at small temperatures and are generally molecular instead of atomic. We therefore need to estimate the value of γ in cool molecular gas. A few previous attempts in this direction are summarized by Larson (1985, Fig. 2) who suggests $\gamma \approx 0.7$ in the absence of stellar heating, for $T \sim 10 - 50$ K and $n \sim 10^1 - 10^5$ cm⁻³. However there are a number of possible heating mechanisms, and the cooling is complicated by the contribution of different coolants and optical depth effects at large densities.

A major study of interstellar cooling and heating at low temperatures (< 100K) was given by Gold-

smith and Langer (1978, hereafter GL) for the density range 10²–10⁵ cm⁻³. The resulting cooling function is dependent on the prescribed abundances of coolants and the treatment of radiative transfer (escape probability method with constant large velocity gradient). A considerably more detailed treatment of the cooling function was presented by Neufeld, Lepp, and Melnick (1995, hereafter NLM) for densities 10³–10¹⁰ cm⁻³ and temperatures 10–2500K. Besides including more coolants, using updated data on cross sections, and a modified velocity gradient parameter for the radiative transfer, NLM obtained coolant abundances by a self-consistent (but steady-state) solution to a large chemical reaction network. The results assume complete shielding from ultraviolet radiation, and may be significantly different in lower-column density regions. We base the following discussion of γ on the results of GL and NLM, concentrating on densities 10²–10⁵ cm⁻³ and temperatures 10–100 K. We emphasize that our purpose is not to give a comprehensive treatment of the cooling and heating functions, but only to outline what seem to be the dominant physical effects on γ and to motivate a more detailed treatment.

For temperatures less than about 100 K, we find that the temperature dependence of the cooling function, parameterized by $L \sim T^b$, can be adequately represented by a density-dependent function, based on Table 4 of GL,

$$b = \frac{1}{2}(1 + \log n) \quad (14)$$

for $\log n$ in the range 2 to 5, where n is the total particle density. The numerical and graphical results presented by NLM are not sufficient to confirm this relation, although the trend of larger temperature dependence at larger densities seems to hold for densities up to 10⁵ cm⁻³, based on Fig.2 in NLM. At smaller densities, based on the data in GL, b is smaller than given by eq. (14). For example, at $n = 10^1$ cm⁻³, $b \approx 0.5$.

For densities less than a few hundred cm⁻³ the total cooling rate per unit volume varies with the square of the density ($c = 2$), but at densities around 10³ cm⁻³ or larger, the density dependence becomes much weaker because of radiative trapping (e.g. GL). The density at which the flattened density dependence occurs depends on a number of effects, but is about 10³ cm⁻³ for the parameters adopted by GL. The resulting density dependence is uncertain because of the approximate nature of the radiative transfer calcula-

²Actually, the range of cooling functions described in sec. 2 give $\gamma = 3.3$ for $10^5 \leq T < 4 \times 10^7$ K. However, those temperatures are never reached in the simulations.

tions in the available work and the assumption of a smooth (not turbulent) velocity field. Inspection of Fig. 3 of NLM indicates that for n between 10^3 and 10^5 cm^{-3} , c is about 1.6 for $T = 100 \text{ K}$ and 1.2 for $T = 10 \text{ K}$, although at $T = 10 \text{ K}$ c is very close to 1.0 for their singular isothermal sphere model. For reasons we do not completely understand, the density dependence exponents at high densities are smaller by about 0.6 in the calculations of GL, Figs. 7a–c, with c as small as 0.5 at $T = 10 \text{ K}$. Some possible reasons for the differences between GL and NLM are given by NLM, although they do not explicitly discuss the differences in density dependence. For illustrative purposes we will adopt $c = 1.2$ for $n > 10^3 \text{ cm}^{-3}$ and $T = 10 \text{ K}$.

The heating rate is problematic because it is uncertain what the dominant process is (see GL, Black 1987, and Hollenbach 1988 for reviews). It is often assumed that the main heating agent is cosmic rays, with $\Gamma \sim \rho$, so that $a = 1$. The heating due to H_2 formation on grains depends on the fraction of neutral hydrogen, but at large densities the heating rate is again proportional to ρ . Heating rates due to gas-grain collisions, compression or collapse, ambipolar diffusion, or turbulence are more complicated and uncertain, and may include a temperature dependence. We ignore these sources here, except to note that b may be significantly larger than unity for these cases. An extreme case is gas-grain heating, which is proportional to $\rho^2 T^{1/2} (T_{gr} - T)$, where T_{gr} is the grain temperature. This case is discussed below.

Our results suggest different behavior of γ in four density ranges.

1. $n < 10^3 \text{ cm}^{-3}$. In this case, taking the density dependence of the heating as $a = 1$, and including the density dependence of b (eq. [14]) in eq. (13), an effect that pushes γ closer to unity, the polytropic index is 0.56 for $n = 10^2$ ($b = 1.5$) and 0.88 for $n = 10^3$ ($b = 2$). These bracket the estimate by Larson (1985). At densities as low as 10 cm^{-3} , $b \approx 0.5$ based on the GL cooling rates, and γ is negative, corresponding to thermal instability.

We conclude that, as long as the dominant heating mechanism is cosmic rays, H_2 formation, or some other process whose rate scales with the density in a manner not much steeper than linearly, the polytropic index will be sufficiently smaller than unity in molecular regions with $n < 10^3 \text{ cm}^{-3}$ that the power law density pdfs found in the simulations should apply there, also. A lognormal pdf should only obtain for

a nearly quadratic density dependence of the heating rate per unit volume.

2. $n \sim 10^3$ to a few times 10^4 cm^{-3} . The situation is different at densities larger than 10^3 cm^{-3} , at least when gas-grain collisional cooling does not dominate, because radiative trapping weakens the density dependence of the cooling rate, i.e. reduces the exponent c . At $T = 10 \text{ K}$, adopting $c = 1.2$ from the results of Neufeld et al. (1995) and again using $a = 1$ for the density dependence of the heating rate, γ varies from 0.98 at $n = 10^3$ to 0.99 at $n = 10^5$. At $T = 100 \text{ K}$, taking $c = 1.6$, γ varies from 0.92 to 0.97 over this density range. The polytropic indices are close enough to unity that the lognormal density pdf might occur. There is some inconsistency in arriving at these numbers, because the density dependence of the temperature exponent in the cooling rate (eq. 14) was based on GL, while the density exponent is based on NLM. Without the density dependence of γ , the derived values of γ are slightly smaller, but still close to unity.

That γ may be very close to unity at densities above 10^3 cm^{-3} is by no means a definitive result. After the above calculations were done, we found that Lis & Goldsmith (1990) have given polynomial fits to the cooling function of GL, which includes radiative trapping. Taking analytical derivatives of their expressions in order to evaluate γ , and assuming a linear dependence of the heating rate on density, we find that at $\log n = (2, 3, 4)$ $\gamma = (0.89, 1.21, 1.26)$. This suggests that γ will only be very close to unity in a narrow density range around 300 cm^{-3} . The reason for the difference is that the effective values of c , the density dependence of the cooling rate, are continuously varying and significantly smaller than the value $c = 1.2$ which we estimated for the high-density cooling functions of NLM.

Based on the NLM cooling rate, we suspect that a major transition occurs at densities above which radiative trapping in the cooling lines becomes important. At smaller densities the polytropic index should be significantly smaller than unity, and a power law density pdf should occur. At larger densities the value of γ should be close to unity, and a lognormal density pdf is possible. Since these different density pdfs are a reflection of the velocity field (which generates density fluctuations through the dilatation $\nabla \cdot \mathbf{u}$), we expect that the velocity field and other associated phenomena should also be qualitatively different in the two density regimes. One caveat to this conclusion is that

radiative trapping may be very different for a turbulent velocity field than for the linear velocity gradients assumed in the existing cooling rate calculations. (For a calculation of molecular line formation in a turbulent velocity field, but without density fluctuations, see Kegel, Pielher & Albrecht 1993.) Another caveat is the fact that we obtain values of γ significantly larger than unity for $n = 10^3\text{--}10^4\text{ cm}^{-3}$ using the fits of Lis & Goldsmith (1990) to the cooling function of GL, as discussed above.

The possibility that γ may be close to unity at densities between 10^3 and 10^4 cm^{-3} is consistent with the near constant temperature $\sim 10\text{ K}$ observed in dark clouds without internal protostellar heat sources. However, this latter result is based largely on CO observations that sample a fairly narrow range of densities. Often this result is ascribed either to the efficiency or the temperature dependence of the cooling; however it is clear that near isothermality should occur in this density range primarily because the density dependence of the cooling rate changes as radiative trapping becomes important.

3. $n \gtrsim 10^4\text{ cm}^{-3}$. At still larger densities, a different physical effect becomes important. If there are no embedded protostellar sources to heat the dust grains, then cooling by gas-grain collisions should dominate the molecular cooling at densities above $1 \times 10^4\text{ cm}^{-3}$ to $5 \times 10^4\text{ cm}^{-3}$, depending on the grain temperature and grain parameters. (For the gas-grain energy transfer rate, see, for example, GL and Hollenbach and McKee 1989.) The gas-grain cooling rate is proportional to $\rho^2 T^{1/2} (T - T_{gr})$, so $c = 2$ and $b \approx 3/2$ if $T \gg T_{gr}$. In this case $\gamma \lesssim 1/3$ and so a return to a power law density pdf should occur for densities above $(1 - 5) \times 10^4\text{ cm}^{-3}$. However the grain, and hence gas, temperature is limited by the cosmic background radiation to $T \approx 3\text{ K}$, so it may be difficult to detect the decrease in gas temperature in this density range.

If embedded protostellar sources are present, the grain temperature will probably exceed the gas temperature and gas-grain collisional heating will dominate cosmic ray heating at large densities, as originally emphasized by Goldreich and Kwan (1974). In this case it is easy to show that γ should be significantly *larger* than unity at high densities. For example, at $n = (10^4, 10^5)\text{ cm}^{-3}$, $\gamma = (1.4, 1.3)$, assuming $c = 1.2$ and $T_{gr} \gg T$, and including the uncertain density dependence of the cooling function in eq. (13). These results are uncertain because a reliable treat-

ment of the grain temperature requires a radiative transfer calculation.

4. Extremely large densities. As pointed out by Lis & Goldsmith (1990) and others, the gas-grain coupling at very large densities is so strong that the gas temperature will simply follow the grain temperature, while the latter is controlled by the radiation field. So $\gamma = 1$ may obtain at very large densities when embedded protostars are present, if the ambient radiation field is not coupled to the local gas density. If positive feedback between density and star formation rate exists, then the local ultraviolet energy density will scale similarly. The resulting grain temperature is only a weak function of energy density, scaling roughly with the $1/5$ power. For example, if the local star formation rate per unit volume scaled with the square of the density, $\partial \log T / \partial \log n$ would be 0.4 and γ would be 1.4. Accurate observational determinations of the gas temperature and density in high-density clouds could resolve the issue.

A final remark is in order. It is well known that the Coriolis force (e.g., Binney & Tremaine 1987) and the magnetic field (e.g. Shu, Adams & Lizano 1987; Mouschovias 1987) may act against gravitational collapse. In fact, Vázquez-Semadeni et al. (1996) noted that inclusion of these effects restores a “higher- γ ” behavior to the numerical simulations, when considering the ability of the flow to collapse gravitationally. However, the fact that in the present paper the density pdfs of simulations including both these effects still exhibit power-law tails on their high-density sides suggests that the local production of large turbulent density fluctuations generated by the stellar energy input is not strongly inhibited by these processes. The effective compressibility of the flow probably still has an equivalent polytropic exponent significantly smaller than unity.

4. Applications

4.1. Can the density pdf be used to derive the stellar IMF?

Padoan, Nordlund, and Jones (1997, PNJ) have attempted to derive the mass spectrum of collapsing gas clouds from the density pdf of simulations. The procedure is as follows. If $f(\rho)$ is the density pdf, then $g(\rho) \sim \rho f(\rho)$ is the fraction of mass at a given density. Assuming that objects collapse if their mass exceeds the Jeans mass M_J , proportional to $\rho^{-1/2}$, they propose that the fraction of collapsing structures of mass

$< M$ is proportional to $\int_{\rho_J}^{\infty} g(\rho)d\rho$. The IMF is then the distribution of Jeans masses, obtained by differentiating this integral, giving an IMF proportional to $g(\rho)d\rho/dM_J$. Since $d\rho/dM_J \propto M_J^{-3}$, this gives an IMF which is an M^{-3} power law multiplied by the density pdf expressed in terms of Jeans mass, which they find from numerical simulations to be a lognormal. This latter factor is Gaussian in $\ln M^2$, with a mean that depends on the temperature and turbulent velocity dispersion. This dependence causes the logarithmic slope of the IMF to depend on these parameters. In principle this procedure could be applied to any density pdf, such as those discussed above. Our concern here is the validity of using a one-point density pdf to derive a distribution of masses, since mass as an attribute implies a coherent, contiguous “object” or structure, while the density pdf contains no spatial information of this nature. The problem is basically that not just any region of a given density can form a collapsing object, it must have a *size* large enough to contain a mass corresponding to at least the Jeans mass at that density.

The problem can be illustrated using a specific example. Since $M_J \propto \rho^{-1/2}$, the largest mass objects should form where the density is smallest. The lowest density regions are the “valleys” or “voids” in the density field. Imagine the density field as an array of pixels. If we consider a density value far into the low-density tail of the density pdf, a lognormal form of the pdf indicates that only a small fraction of pixels can have such small densities, and there is no *a priori* reason to think that these pixels will be sufficiently contiguous that there really exists a coherent region of that density large enough to contain the corresponding Jeans mass (or any specified mass). In other words, in order to collapse, these low-density pixels must be spatially connected such that they form a very large low-density region. In general we expect the low density valleys to be scattered through the density field in some way. A Jeans’ mass worth of matter centered at the position of a low-density pixel would be expected to contain pixels of a range of densities, some very large. This inconsistency occurs at any density—the low density case is just a severe example. Even at pixels where the density is largest, so the Jeans mass will be smallest, there is no reason to assume that nearby pixels out to mass M_J will be at that density.³ These same remarks apply to other

instability criteria (since it is not at all clear that the thermal Jeans mass plays any role; e.g. Wiseman & Adams 1994; Simon 1997; Chappell & Scalo 1997).

PNJ apparently recognized this problem, and state that 99% of the density *peaks* in their simulations contain mass exceeding the Jeans mass. However, our concern here is that, according to the formulation used by PNJ, the high-mass portion of the IMF, which is the region of most interest, is determined by *low-density* side of the density pdf. The problem then is that the low-density part of the pdf corresponds to *voids* in the density distribution, not peaks, and these low-density regions would have to be coherent over extremely large scales to contain a Jeans mass (which is largest at smallest densities). Furthermore, it is well-established observationally that stars form in the *peaks* of the density distribution (i.e., the clouds), not the voids. The implication that the highest-mass stars form in the lowest-density regions contradicts a large body of evidence on local star-forming complexes showing that high-mass stars form preferentially in the *densest* regions (e.g. compare Orion and Taurus, or the spatial distribution stars by luminosity within individual clusters in Orion and other regions that contain massive stars).

Yet another concern is the statement itself by PNJ that the vast majority of their density peaks is Jeans-unstable, since it has been suggested on both observational (e.g., Falgarone, Puget & Péault 1992; Magnani, LaRosa & Shore 1993) and numerical (Vázquez-Semadeni et al. 1997) grounds that a large fraction of the turbulence-induced transient density fluctuations are not gravitationally bound. Besides, PNJ’s simulations are not reported to be self-gravitating, so the statement that the density peaks are unstable appears inconsistent.

We conclude that the one-point density pdf cannot be used to derive a mass function of “clouds” or protostars: spatial statistics are necessary. One might consider the two-point density pdf, which gives the probability that pairs of points separated by r have densities ρ_1 and ρ_2 . A second-order moment of this two-point probability distribution, the corre-

Semadeni’s (1994) criterion for the development of hierarchical structure based on the density pdf (A. Noulez, private communication). Nevertheless, in that work, an additional constraint was required from the density pdf, namely, that it exhibited self-similarity as smaller and smaller regions are considered. This requirement may possibly provide the necessary spatial information.

³ A similar problem has been pointed out about Vázquez-

lation function, reduces this information greatly (in the same way that the variance reduces the one-point pdf to a single number). But even the 2-point pdf is insufficient to estimate the mass spectrum because we need to know the probability that there exists a region with enough contiguous pixels in a given density range to comprise a mass sufficient for instability. At the least, a joint probability distribution of densities and coherence sizes would be needed, but construction of this joint distribution is equivalent to directly constructing the mass spectrum from the simulations or observational data. The plausibility of our conclusion can also be seen by considering the process of estimating a mass spectrum for interstellar “clouds” from observational data. Within an arbitrary density field (or a three dimensional field with radial velocity as one axis, as for spectral line data) the identification of entities defined in some operational manner and the measurement of their attributes is a complicated and subjective procedure (e.g. Houlahan and Scalo 1992, Williams et al. 1994), while the estimation of the column density pdf by histogram construction for the same field is simple by comparison. This difference in computational effort is a reflection of the essential role of spatial information in the former procedure and the absence of such information in the latter.

It is interesting to note that the procedure proposed to derive the mass spectrum of bound condensations by PNJ is very similar in approach to the derivation of the mass spectrum of bound objects in a gaussian density field (in the linear regime) used in considerations of galaxy formation (e.g. Press & Schechter 1974, Peacock & Heavens 1990). There the threshold density is taken as the critical density contrast needed at some initial time so that the contrast will be about unity at a later time. But in the cosmological case, the derivation assumes that the density field is successively smoothed by window functions of scale R , which would correspond to a mass M proportional to the mean density in the window. This smoothing takes care of the problem discussed here, of having enough extent at each critical density to contain mass M , but the answer, even for a gaussian random field, depends on the power spectrum and the rather arbitrary choice of window function. In the case of simulations the problem is more difficult. In particular, we suspect that because the density field is non-gaussian, the answer will depend on higher-point correlations, as we speculated earlier.

In any case, using simulations alone, we think that

the only way to determine the mass spectrum of coherent condensations, whether collapsing under the Jeans criterion or not, is to directly identify “clouds” in the simulation and calculate their frequency distribution (e.g. Vázquez-Semadeni et al. 1997; Chappell and Scalo 1997). There is no “shortcut” to the IMF through the one-point density pdf.

Besides the conceptual problem of deriving an IMF from the one-point density pdf without spatial information, the IMF derived by PNJ does not give a good representation of the observed IMF in either field stars, open clusters, OB associations, or nearby galaxies. The PNJ IMF decreases with increasing mass with a power law index that decreases (becomes more negative) with increasing mass. PNJ recognized that the function does not match the observed IMF at any single gas temperature and velocity dispersion, and so attempted to remedy the situation by assuming a T^{-1} distribution of gas temperatures between 5 and 40 K and showed that such a temperature distribution could approximately match the Miller & Scalo (1979) field star IMF. The problem is that the Miller-Scalo IMF at higher masses has long been superseded by a large body of observations (see Scalo 1986 for a summary of work before 1985; also Rana 1991 for field stars, Massey et al. 1995a, b for massive stars in the Galaxy and Magellanic Clouds; see Scalo 1997 for a recent review) that suggest that for masses above about $1.5 M_{\odot}$, the IMF is not lognormal, but is best fit by a power law of slope around -1.7 ± 0.2 with (probably) a flatter high-mass tail. Such a form would be difficult to produce from the PNJ formalism without a very contrived mixture of gas temperatures and velocity distributions.⁴

For the above reasons, we must conclude that the application of the PNJ IMF to globular clusters (Padoan, Jimenez, and Jones 1997), low surface

⁴For comparison, if the density pdf were a power law of the form $f(\rho) \sim \rho^{-\theta}$, with a sharp cutoff at small densities, the IMF for a single-temperature Jeans mass would be proportional to $M^{2\theta-5}$, or $M^{-1.6}$ for $\theta = 1.7$ as found here, in good agreement with observations. The flattening at large masses could be provided by the flattening of $f(\rho)$ at densities near the peak. The turnover of the IMF at small masses could be ascribed to “turbulent viscosity” steepening the density pdf at large densities (which requires $\theta > 2.5$ in this regime if it were a power law). By assuming a parameterized distribution of temperatures, we could match essentially any desired form of the IMF. However we emphasize that this procedure is unwarranted, and only give the example as an illustration of the ease with which such a parameterized IMF model could produce a match to any set of observations.

brightness galaxies (Padoan, Jimenez, and Antonuccio-Delogu 1997), and other galaxy evolution problems (Chiosi et al. 1997) are without basis. The galaxy evolution models of Chiosi et al. (1997) do represent a major advance in such modelling, in that the coupling between the IMF and the energy equation is explicitly treated. However we interpret their results as showing that an IMF that favors higher mass stars for some combination of lower mean gas density and higher temperature and/or velocity dispersion can account for a number of observed chemical and photometric constraints for elliptical galaxies. We only point out that there is as yet no physically consistent model for such an IMF and that other models besides the PNJ model could be constructed to give similar dependences.

We emphasize that the fact that a theoretical formulation of a problem has a large enough number of adjustable parameters to interpret a number of diverse phenomena is not a measure of its physical validity. A theoretical IMF that can be applied to these and other problems must be able to give a natural account of contemporary studies of the local field star and cluster IMF, and, besides, cannot be derived solely from the density pdf. A brief summary of recent theoretical models for the IMF is given in Scalo (1997).

4.2. Applications to Column Density Statistics

Our critique of the PNJ IMF does not extend to their interpretation of the increase of extinction standard deviation with average extinction found by Lada et al. (1994), given by Padoan, Jones, & Nordlund (1997). We agree that this increase constrains the density pdf and probably requires an intermittent tail (not necessarily lognormal, though) and a power spectrum of the density field $P(k) \propto k^x$, with x around -2 to -3 . However, whether or not simulations with different physical assumptions can give the requisite intermittency and power spectrum remains an open question. We have examined the power spectrum of a 2-dimensional MHD model (fig. 12) and find a small intermediate range of wavenumbers over which the power spectrum is a power law with index around -2.4 , close to the value of -2.6 reported by Padoan, Jones, and Nordlund (1997) in their simulations, although a much flatter and just as extensive power law occurs at smaller wavenumbers in the present simulations. A more direct test of the simulations would

be an estimate of the pdf of column densities. Such a comparison, using IRAS $100\ \mu\text{m}$ column densities for low-mass star regions and ^{13}CO data for high-mass star regions, is postponed to a separate paper (Scalo, Chappell, Miesch, and Vázquez-Semadeni, in preparation).

Note that in our simulations, the wavenumber range with a -2.6 “slope” may actually constitute the range at which the mass diffusion is active, producing an extended exponential decay which may be confused with a power-law. This effect could also be at work in the simulations of Padoan, Jones, & Nordlund(1997), due to the numerical diffusion. Note, however, that this cannot be at the origin of the power-law tails we observe in the density pdfs from our simulations, since the effect of the diffusion term is to *smooth out* fluctuations, while the power-law tails in the pdfs are *enhancements* over the lognormal alternative.

4.3. Size distribution of wind-driven shells

Shells driven by H II regions, protostellar winds, supernova remnants (SNRs), and superbubbles are believed to play an important role in shaping interstellar structure over a range of size scales, and the velocity and size distributions of such shells are of interest in a variety of astrophysical contexts, such as the porosity of the ISM (Oey & Clarke 1997) and models for the IMF (Silk 1995). The expansion law for shells depends on the ambient interstellar density, so a distribution of ambient interstellar densities could affect the predicted size and velocity distributions. The distribution of sizes of SNRs and superbubbles for a distribution of source luminosities has been treated in detail by Oey & Clarke (1997), who assumed a constant ambient density. Here we illustrate the role of a density pdf by assuming a constant luminosity. For simplicity, we neglect the effect of shell stalling which occurs when the driving pressure matches the ambient pressure. We are mostly interested in effects that occur in molecular clouds subjected to internal protostellar winds. In this case the appropriate expansion law is probably that for a non-adiabatic momentum-conserving shell (see the conditions derived in Norman & Silk 1980), which can be expressed as

$$R \sim L^{1/4} \rho^{-1/4} t^{1/2}, \quad (15)$$

where L is the source luminosity, which we assume is constant for illustrative purposes, and R the radius of the shells.

For a constant star formation rate B , the size distribution for a given ambient density is given by $N(R, \rho)dR = Bdt$, so, integrating over the pdf of ambient densities,

$$N(R) \sim \int_{\rho_1}^{\rho_2} f(\rho) (dR/dt)^{-1} d\rho. \quad (16)$$

If the ambient densities were the same for all sources ($f(\rho)$ a delta function), then, since eq. (15) gives $(\partial R/\partial t)^{-1} \sim R$, $N(R)$ would scale as R , reflecting the larger number of shells at small velocities. For the case of a distribution of ambient densities, the integration limits require some care. We assume that the lower and upper limits of ambient densities are ρ_{min} and ρ_{max} , and that all the sources are only active for a time t_e . Then for radii R less than some small $R = R_1$, all ambient densities, even up to the maximum density, allow expansion to radius R in a time t_e . But for larger radii, shells expanding into high density material will not reach that size in time t_e , so the limits of integration are ρ_{min} to $\rho(R, t_e)$, where $\rho(R, t_e)$ is the ambient density for which a shell will reach size R within time t_e . So

$$N(R) \sim \int_{\rho_{min}}^{\rho(R, t_e)} f(\rho) \rho^{1/2} R d\rho. \quad (17)$$

Taking $f(\rho) \sim \rho^{-\theta}$ gives

$$N(R) \sim \left[\rho(R, t_e)^{-\theta+3/2} - \rho_{min}^{-\theta+3/2} \right] R. \quad (18)$$

For $\theta > 3/2$ (steeply declining pdf), most of the ambient material is at small ρ , and the second term dominates. The size distribution is then unaffected by the density pdf, $N(R) \sim R$, because the pdf is in effect a delta function.

But if $\theta < 3/2$ (flatter pdf), the first term dominates. Since $\rho(R, t_e) \sim R^{-4}$ for a fixed t_e , the resulting size distribution is

$$N(R) \sim R^{4\theta-5}. \quad (19)$$

For $\theta < 3/2$, $4\theta-5 < 1$, so $N(R)$ increases less rapidly than R ; shells at small R become significant because more of the ambient material is at large densities. The same derivation for an adiabatic pressure-driven shell (Weaver et al. 1977) gives $N(R) \sim R^{5\theta-8/3}$ for $\theta > 2/3$.

The situation is actually much more complicated for a number of reasons. The density pdfs found in

the simulations are strongly decreasing functions of ρ for large densities, but increasing, and extremely uncertain, functions of ρ at small densities. Numerical integration of eq. (17) for a double power-law or lognormal density pdf would be a useful exercise, but our purpose here is only to illustrate the potential effect. Secondly, a distribution of source luminosities should be included (i.e. a generalization of Oey & Clarke's 1997 result to include the density pdf). Third, as noted above, shell interactions are probably important (see also Norman & Silk 1980), and for this process the effect of a distribution of ambient densities would be to affect the column density and velocity distributions of the interacting shells. Finally, we note that the present derivation suffers from the same lack of spatial information that we claimed precludes a derivation of the mass spectrum. If the ambient density fluctuations were all on scales smaller than any shell size of interest, then the effect of the density distribution would only be to corrugate the shell in some irregular manner, as different parts of a given shell expand into different ambient densities. On the other hand, some coherent density fluctuations in the ISM have scales larger than the shell sizes of interest. A full examination of these problems is beyond the scope of the present paper.

4.4. Comparison with cosmological simulations

It is of interest to compare our results with cosmological simulations of the evolution of density fluctuation in the universe. Such calculations usually contain a minority of the matter in baryonic form, with the rest either in “cold” or “hot” dissipationless particles meant to represent varying dark matter candidates, or some combination of the two. The dissipationless component is equivalent to a self-gravitating Burgers flow (no pressure, $\gamma = 0$) with viscosity arising only from numerical diffusion, while the coupled baryonic component follows the Navier-Stokes equation with self-gravity.

Most of the work in this field has been aimed at using the density pdf as a discriminator of parameters related to initial conditions, such as the index of the initial power spectrum or deviations from initial Gaussian statistics. Several papers, apparently beginning with Hamilton (1985), have proposed that the density pdf in the not-too-strongly nonlinear regime is lognormal (see Weinberg and Cole 1992, Kofman et al. 1994, Bernardeau and Kofman 1995; for other

references see Protogeros and Scherrer 1997). However Bernardeau and Kofman (1995) argued that it is likely that the lognormal distribution only obtains for an initial power spectrum with index not too different from -1 (as in cold dark matter scenarios) and for a variance of the (smoothed) density field not too large (less than around unity). For conditions outside of this range the density pdf appears to have a power-law, not lognormal, high-density tail (Bouchet and Hernquist 1990, Melott et al. 1997; these power laws are to be distinguished from the steeper power laws that result from caustics in the Zeldovich approximation with no smoothing). Although in general such simulations are not isothermal and in some cases refer to pressureless dark matter, the apparent transition from lognormal at small density variance to power law at larger density variance may be understood as the analogue of the Mach number dependence described in the present paper, the range of density values being just too small for the power-law range to develop.

A recent discussion of a cold-plus-hot dark matter simulation that presents the density pdf has been given by Klypin, Nolthenius, and Primack (1997). These simulations use a particle-mesh code with a force mesh resolution of 512^3 in three dimensions. The resulting function $\rho f(\rho)$ (their fig. 16) shows a clear power-law over more than two orders of magnitude in density, with a power-law index of about -1.2 , and a dropoff at the highest densities due to finite resolution. There is certainly no hint of a lognormal form. The result supports our contention of a power law density pdf driven by advection, and shows that power-law behavior occurs even in three dimensions. The power law index is steeper than found here by about 0.2 to 0.6 , but it is uncertain whether this is a result of the different dimensionality, the fact that the self-gravity is mainly supplied by the dissipationless component, or some other effect.

5. Conclusions

In this paper we have discussed various theoretical aspects of the density probability distribution function, or pdf, of the ISM. We first presented evidence that the pdf appears to be a power-law at high densities in a number of two-dimensional numerical simulations of the ISM at intermediate scales, in which the various intervening physical agents are progressively removed until only the nonlinear advection operator of the momentum equation is left. Additionally, in all

cases the morphology is extremely filamentary. This result has two main implications. First, it suggests that both the functional form of the pdf and the morphology of the density field are the signature of the advection operator.

Second, this result is in contrast with previous findings that the pdf is lognormal (Vázquez-Semadeni 1994; Padoan et al 1997 a, b, c). To resolve the discrepancy, we turned to the one-dimensional simulations of PVS, which suggest that the lognormal pdf is realized only in the isothermal case ($\gamma = 1$), while at smaller values of γ a power law appears. Moreover, PVS report that the deviation from a lognormal is larger at larger Mach numbers. These results are consistent with the fact that the simulations of Vázquez-Semadeni (1994) and Padoan et al. (1997a, b, c) were isothermal, while those presented here in all cases have small or zero values of γ .

The dependence on the polytropic index γ prompted an investigation on what are its expected values in the actual ISM, as determined by the equilibrium between heating and cooling rates, which in turn depends on the density and temperature of the medium. From inspection of published heating and cooling rates, we expect that at densities below $\sim 10^3 \text{ cm}^{-3}$ values of γ significantly smaller than unity should occur, while at larger densities, values near unity should appear. The switch-over occurs because of the effect of radiative trapping in decreasing the density dependence of the molecular cooling rate at densities above $\sim 10^3 \text{ cm}^{-3}$. At densities larger than around 10^4 cm^{-3} gas-grain collisional cooling or heating should dominate, forcing γ back away from unity. Thus, lognormal pdfs are only expected in the range 10^3 to $(1 - 5) \times 10^4 \text{ cm}^{-3}$, with power law pdfs outside of this range of densities. However, at extremely large densities the gas-grain coupling may be so efficient that the gas temperature will simply follow the grain temperature which is controlled by the ambient UV radiation field. To the extent that the radiation field energy density is independent of the gas density, the temperature will then be constant, so a return to a lognormal density pdf may occur at such large densities. A star formation rate-density coupling would increase γ somewhat above unity through the effect of the young massive stars on the grain temperature.

A number of possible applications were discussed. Most importantly, we discussed the feasibility of deriving the mass spectrum of bound condensations or the stellar IMF from knowledge of the density pdf

alone, as recently done by PNJ. We conclude that this is not possible, because the pdf does not contain spatial information, while the gravitational instability criterion requires simultaneous knowledge of mass and size information. Second, we briefly discussed the applicability to extinction statistics (Padoan, Jones & Nordlund 1997). Third, we analyzed the effect of an inhomogenous density field on the size distribution of wind-driven shells in the ISM. We find that in a simple example case with $f(\rho) \sim \rho^{-\theta}$, the resulting distribution increases more slowly with shell size than in the case of a uniform density background if $\theta < 3/2$. However, we warn that the real situation is likely to be much more complicated.

Finally, we compared our results with those from a number of cosmological simulations, in which both lognormal and power-law forms of the pdf have been reported. We speculate that the appearance of lognormal pdfs for non-isothermal situations may be a consequence of small density variances, analogous to the Mach number effect described here.

A central result of our work is the conclusion that it is primarily the nonlinear advection operator operating on a source of compressible motions (whether it be self-gravity or nonlinear waves or cooling or something else) that is responsible for both the general filamentary morphology (which would include sheets in 3D) and for the power law portion of the density pdf. This result is consistent with the presumed tendency of the advection term to induce multiplicative processes which lead to power law scaling, as it does in the incompressible case. If this is correct, then the simulations studied here should lead to investigations of analytical models for the behavior of the advection operator in a highly compressible medium. For that purpose our simulations provide a constraint in the form of the density pdf that must be explained both when γ is and is not close to unity, as well as a constraint on the morphology. As an example, we point out that Elmegreen's (1997) construction of a fractal by nesting can be shown to produce a density pdf that has the form $f(\rho) \sim \rho^{-2}$, independent of fractal dimension, which is not much different from the power laws found here. Although Elmegreen's model is a static construction with no reference to underlying physics such as advection, this does suggest that an advection model that is related to hierarchical nesting can explain the power-law density pdf.

Alternatively, the physics might be multiplicative but not involve nesting. For example, the action of

advection could simply be to steepen fluctuations into "shells", or "filaments" or "spikes" (depending on dimensionality), as occurs in the Burgers equation. After one crossing time the evolution is dominated by the merging of these entities (which we might refer to as "blobs"), a process that is described by the so-called "coalescence equation". From much previous work we know that the solution of this kinetic equation, when forced at small scales, is a power law mass spectrum with index around -1.5 to -2 . If the blobs were spikes or filaments or shells whose thicknesses were relatively constant or at least independent of their mass, the density pdf would be a power law in the same range. Obvious variations and elaborations on this theme suggest themselves.

Our point is that it is relatively easy to think of simple models that might explain a power law density pdf. However much more work is needed to understand the actual physics of advection acting on a source of compressibility, and how that physics gives rise to the observed and simulated morphology and statistical properties. Given the longstanding difficulties with the analogous questions in the incompressible case (in which vorticity dynamics plays the key role), we do not expect oversimplified models to provide the necessary answers.

We thank Paul Shapiro and Bruce Elmegreen for useful comments. The HD and MHD runs were performed on the CRAY YM-P 4/64 of DGSCA, UNAM. This work was supported by NASA Grant NAG5-3107 and a grant from Cray Research to J. S. , grants UNAM-DGAPA IN105295 and UNAM/CRAY SC007196 to E. V.-S , a joint CNRS-CONACYT grant to E. V.-S and T. P., and by a grant from the PCMI CNRS program to T. P.

REFERENCES

- Ballesteros-Paredes & Vázquez-Semadeni 1997, in preparation
- Bernardeau, F. and Kofman, L. 1995, ApJ, 443, 479
- Binney, J. & Tremaine, S. 1987, Galactic Dynamics (Princeton: Princeton University Press)
- Black, J. H. 1987, in Interstellar Processes, ed. D. J. Hollenbach & H. A. Thronson (Dordrecht: Reidel), p. 731
- Chappell, D. and Scalo, J. 1997, in preparation

- Chiosi, C., Bressan, A., Portinari, L., and Tantalo, R. 1997, preprint
- Bouchet, F. & Hernquist, L. 1992, *ApJ*, 400, 25
- Elmegreen, B.G. 1991, *ApJ*, 378, 139
- Elmegreen, B.G. 1997, *ApJ*, 486, 944
- Falgarone, E., Puget, J.-L., & Pérault, M. 1992, *A&A*, 257, 715
- Foster, P. N. & Boss, A. P. 1996, *ApJ*, 468, 784
- Goldsmith, P. F. & Langer, W. D. 1978, *ApJ*, 222, 881 (GL)
- Goldreich, P. and Kwan, J. 1974, *ApJ*, 189, 441
- Gotoh, T., & Kraichnan, R. H. 1993, *Phys. Fluids A*, 5, 445
- Hollenbach, D. J. & McKee, C. F. 1989, *ApJ*, 342, 306
- Kegel, W. H., Pielner, G. & Albrecht, M. A. 1993, *AstrAp*, 270, 407
- Klypin, A., Nolthenius, R., and Primack, J. 1997, *ApJ*, 474, 533
- Kofman, L., Bertschinger, E., Gelb, J.M., Nusser, A., & Dekel, A. 1994, *ApJ*, 420, 44
- Lada, C.J., Lada, E.A., Clemens, D.P., & Bally, J. 1994, *ApJ*, 429, 694
- Larson, R. B. 1985, *MNRAS*, 214, 379
- Lis, D. C. & Goldsmith, P. F. 1990, *ApJ*, 356, 195
- Magnani, L., LaRosa, T. N., & Shore, S. N. 1993, *ApJ*, 402, 226
- Massey et al. 1995a *ApJ* 438, 188
- Massey et al. 1995b *Ap*. 454, 151
- Miller, G.E. & Scalo, J.M. 1979, *Ap.J.S.*, 41, 413.
- Mouschovias, T. Ch. 1987, in *Physical Processes in Interstellar Clouds*, ed. G. E. Morfill & M. Scholer (Dordrecht:Reidel), 453
- Neufeld, D. A., Lepp, S., & Melnick, G. J. 1995, *ApJS*, 100, 132 (NLM)
- Norman, C. & Silk, J. 1980, *ApJ*, 238, 158
- Oey, M.S. and Clarke, C.J. 1997, *MNRAS*, in press
- Padoan, P., Nordlund, A., & Jones, B.J.T. 1997, *MNRAS*, 288, 145 (PNJ)
- Padoan, P. & Nordlund, A. 1997, preprint
- Padoan, P., Jimenez, R., & Anotnuccio-Delogu, V. 1997a, preprint
- Padoan, P., Jimenez, R., & Jones, B. 1997b, *MNRAS*, 285, 711
- Padoan, P., Jones, B.J.T., & Nordlund, A. P. 1997c *ApJ*, 474, 730
- Padoan, P. 1995, *MNRAS*, 277, 377
- Passot T., Pouquet A., 1988, *J. Comp. Phys.* 75, 300
- Passot T., Vázquez-Semadeni E., Pouquet A., 1995, *ApJ*, 455, 702
- Passot T., & Vázquez-Semadeni, E. 1997, to be submitted to *Phys. Fluids* (PVS)
- Peacock, J.A. & Heavens, A.F. 1990, *MNRAS*, 243, 133.
- Pongracic, H. 1993, *Mem. S.A.It.* 65(4), 1095
- Press, W.H. & Schechter, P.L. 1974, *ApJ*, 187, 425.
- Protogeros, Z.A.M. & Scherrer, R.J. 1997, *MNRAS*, 284, 425
- Scalo, J.M. 1986, *Fund.Cos.Phys.*, 11, 1.
- Scalo, J.M. 1997, in *The Stellar Initial Mass Function*, Proc. 38th Herstmonceux Conference, ed. G.Gilmore, I.Parry, and S.Ryan, in press.
- Scalo, J.M., Chappell, D., Miesch, M. & Vázquez-Semadeni, E., in preparation
- Shu, F., Adams, F. C., Lizano, S. 1987, *ARAA*, 25, 23
- Silk, J. 1995, *ApJL*, 438, L41
- Simon, M. 1997 *ApJ* (Letters), 482, L81
- Van Leer, B. 1977, *J. Computational Phys.*, 23, 276
- Vázquez-Semadeni, Ballesteros-Paredes & Rodríguez, L. 1997, *ApJ*, 474, 292
- Vázquez-Semadeni, Passot & Pouquet A., 1995, *ApJ*

- Vázquez-Semadeni, Passot & Pouquet A., 1996, ApJ
 Vázquez-Semadeni, E. 1994, ApJ, 423, 681
 Weaver, R., McCray, R., Castor, J., Shapiro, P., &
 Moore, R. 1977, Ap. J., 218, 377
 Weinberg, D.H. & Cole, S. 1992, MNRAS, 259, 652
 Wiseman, J. J. & Adams, F. D. 1994, ApJ, 435, 708

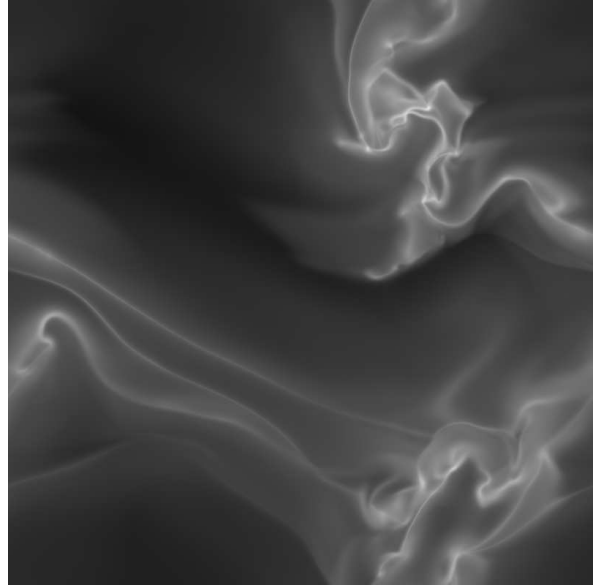


Fig. 1.— Logarithmic grayscale image of the density field of run MHD800 at $t = 1.2t_o$, where $t_o = 8.2 \times 10^7$ yr is the sound crossing time. The simulation represents a region of size 1 kpc, has an initial temperature of 10^4 K, and has an initially turbulent velocity field with an rms velocity fluctuation of 11.7 km s^{-1} . The maximum and minimum values of the density at the time shown are $\rho_{\max} = 526.3$ and $\rho_{\min} = 2.42 \times 10^{-2}$.

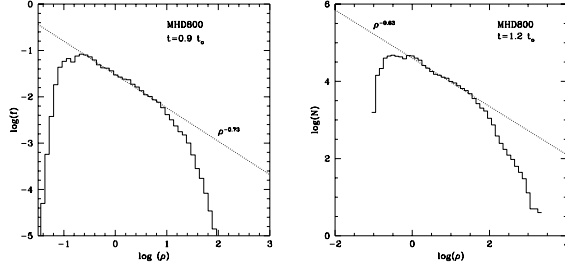


Fig. 2.— Histograms of $\log \rho$ for run MHD800 at a) $t = 0.9t_o$ (left) and b) $t = 1.2t_o$ (right). The localized stellar heating was turned off at $t = 0.8t_o$ in a) and at $t = 1.16t_o$ in b). The density field at the latter time is shown in fig. 1. In a) a clear power law is seen in the range $-0.6 \leq \log \rho \leq 0.9$, with slope ~ -0.73 , while in b) a slightly less well-defined power law is seen for $0 \leq \log \rho \leq 1.5$, with slope ~ -0.63 .

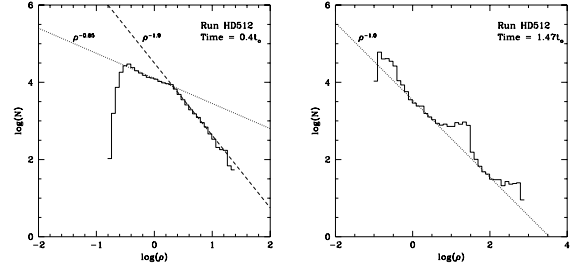


Fig. 4.— Histograms of $\log \rho$ for run HD512 at times a) $t = 0.4t_o$ (left) and b) $t = 1.47t_o$ (right), respectively shown in figs. 3a and b. In a) two power-laws with slopes -0.65 and -1.9 can be seen, although the plot can also be interpreted as a single power law with a bump at $\log \rho \sim 0.3$. In b) a single power law with slope ~ -1.0 is observed, with two bumps, one at $\log \rho \sim 0.7$ and the other at $\log \rho \sim 2.7$. These seem to be respectively due to the onset of star formation at $\rho = 30$ (see text) in the first case, and to the collapsed region, whose peak density is $\rho = 703$.

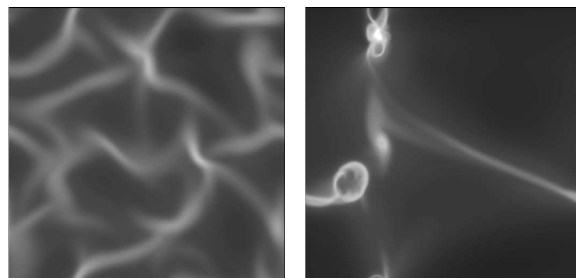


Fig. 3.— Density fields for run HD512 at times a) $t = 0.4t_o$ (left) and b) $t = 1.47t_o$ (right). This is a non-magnetic run otherwise similar to run MHD800 (except for the resolution). In a) a network of filaments is observed, while in b) material in the upper half of the run has collapsed gravitationally. Star formation remained on at all times in this run, although it was not able to avoid the gravitational collapse observed in b).

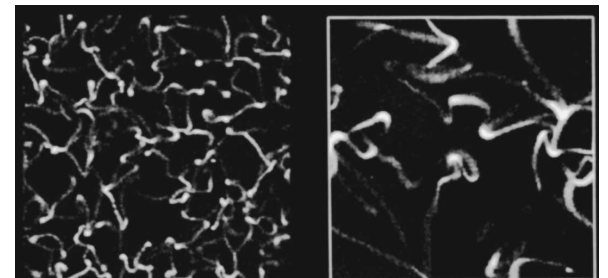


Fig. 5.— Spatial distribution of the square root of the density field at times 0.1 (left) and 10 (right) initial crossing times for a 256^2 quasi-Burgers decay run. The simulation was initialized with a constant density and a velocity field with energy spectrum $E(k) \propto k^4 \exp(-k^2/k_o)$ with $k_o = 8/L$, where L = size of simulation box.

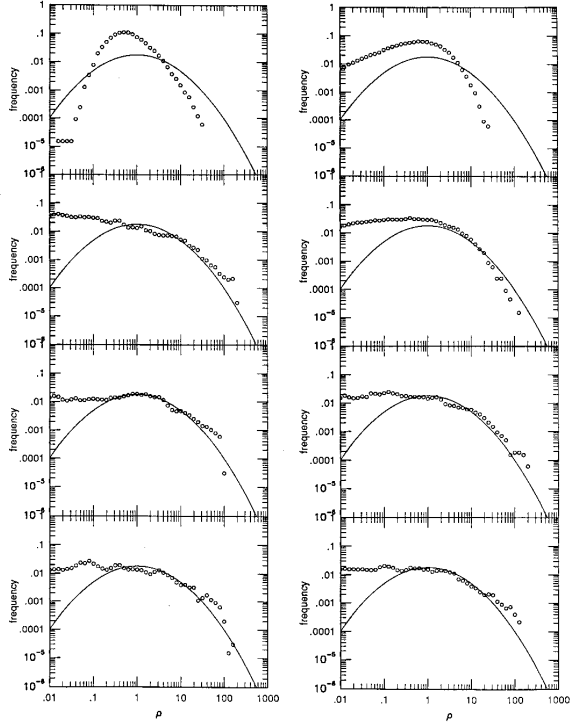


Fig. 6.— Time development (top to bottom) of $\rho f(\rho)$ for two 256^2 quasi-Burgers decay runs. Initial energy spectra are proportional to k^{-2} (left) and k^0 (right). Times, from top to bottom, are 0.006, 0.07, 1.1, and 17 initial crossing times. The solid lines are reference lognormal pdfs with peaks at $\rho = 1$.

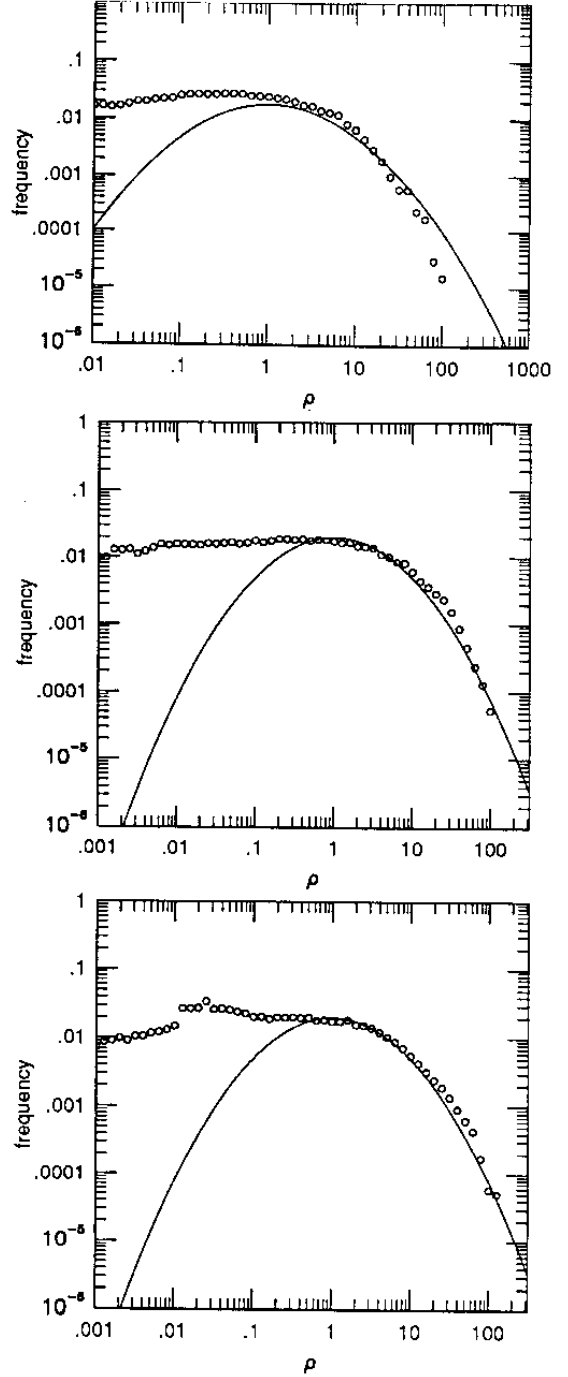


Fig. 7.— Late-time distributions $\rho f(\rho)$ for three 256^2 quasi-Burgers decay simulations initially excited at a single wavenumber $k_0 = 64$ (top), 16 (middle), and 4 (bottom). Solid lines are reference lognormal pdfs with peaks at $\rho = 1$.

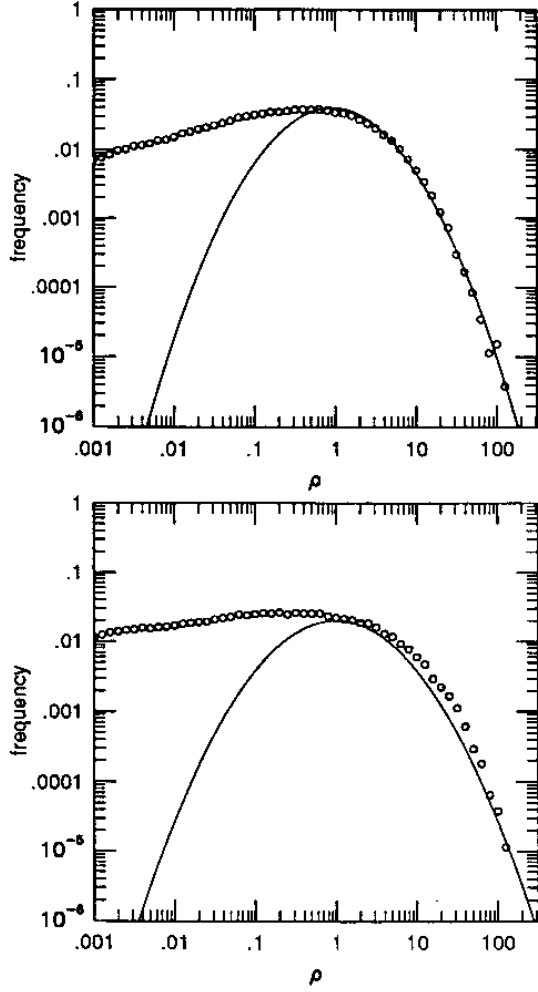


Fig. 8.— Distribution $\rho f(\rho)$ for a 512^2 quasi-Burgers decay simulation at times 0.1 (top) and 2 (bottom) initial crossing times. Solid lines are reference lognormal pdfs with peaks at $\rho = 1$.

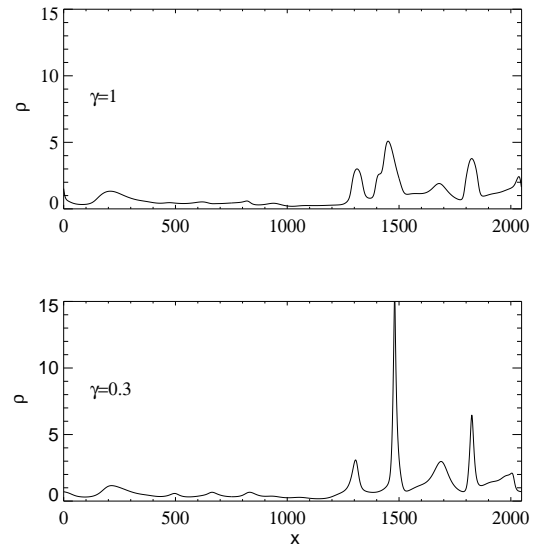


Fig. 9.— Density fields for two one-dimensional runs with $M = 3$ (see eq. [12]), with a resolution of 2048 grid points. a) $\gamma = 1$ (top) and b) $\gamma = 0.3$ (bottom). These runs all start from rest, but are forced with white noise at the large scales (see text) and with a correlation time $t_{\text{corr}} = 4.77 \times 10^{-4} t_o$. The run with $\gamma = 0.3$ shows taller, narrower density peaks than that with $\gamma = 1$.

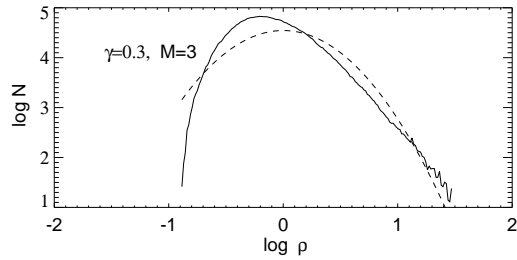
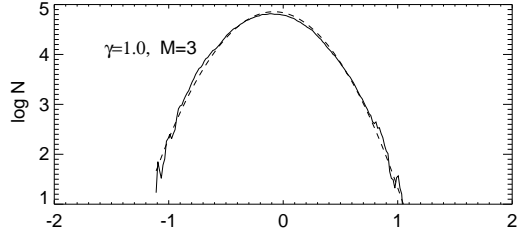


Fig. 10.— Histograms of $\log \rho$ for the 1D simulations shown in fig. 9, with $M = 3$. The runs are sampled at intervals $\Delta t = 1.59 \times 10^{-2} t_o$ over a total time $t = 23.9 t_o$. The histograms thus include 1500×2048 data points. The dotted lines show lognormal fits to the curves. a) $\gamma = 1$ (top). The fit by a lognormal is excellent. b) $\gamma = 0.3$ (bottom). The histogram differs drastically from a lognormal, and instead a clear power-law is seen at high densities, in the range $0.3 \leq \log \rho \leq 1.3$.

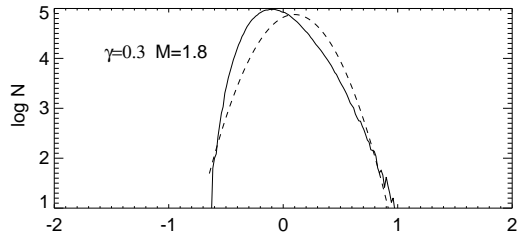


Fig. 11.— Histogram of $\log \rho$ for a 1D simulation similar to that shown in fig. 9a, except with $M = 1.68$. The deviation from a lognormal is seen to be less pronounced than in the case $M = 3$. Also, the power-law at high densities is less well-developed.

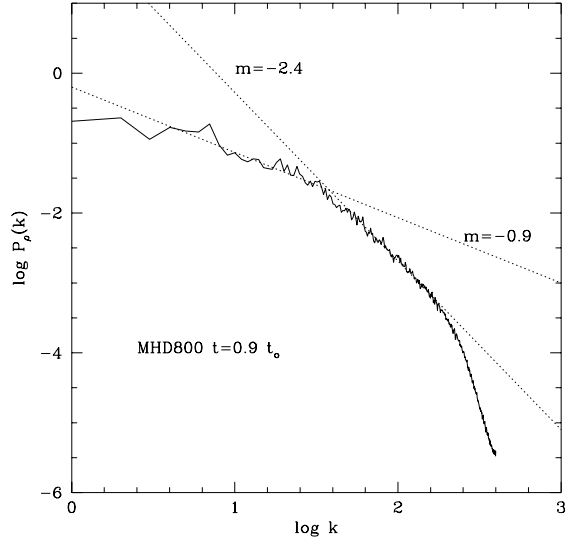


Fig. 12.— Density power spectrum for run MHD800 at time $t = 0.9 t_o$. Two power laws are seen, one in the range $0.6 \leq \log k \leq 1.5$ (k is the wavenumber) with slope ~ -0.9 , and the other in the range $1.5 \leq \log k \leq 2.3$, with slope -2.4 . The region with the steeper slope may actually not be a true power law, but rather a slow exponential decay due to the mass diffusion term in the continuity equation.